Global and Planetary Change 90–91 (2012) 20–28

Contents lists available at SciVerse ScienceDirect

Global and Planetary Change

journal homepage: www.elsevier.com/locate/gloplacha

Tomography of the southern Taiwan subduction zone and possible emplacement of crustal rocks into the forearc mantle

W.B. Cheng [a,*], S.K. Hsu [b], C.H. Chang [c]

[a] Department of Environment and Property Management, Jinwen University of Science and Technology, 99 Ann-Chung Rd., Hsin-Tein District, New Taipei City, Taiwan
[b] Institute of Geophysics, National Central University, Taiwan
[c] Central Weather Bureau, Taiwan

ARTICLE INFO

Article history:
Received 31 December 2010
Accepted 13 January 2012
Available online 20 January 2012

Keywords:
seismic tomography
serpentinization
fluid migration
gravity

ABSTRACT

This paper investigates velocity structure of the active plate boundary in southern Taiwan by joint analysis of gravity anomaly and seismic arrival time data. P and S–P arrival time data from 3238 earthquakes were used. In addition to CWBSN permanent networks, seismic data include the Central Weather Bureau permanent networks and a temporary network consisting of 11 ocean bottom seismometers (OBSs) that was deployed to detect the aftershocks of the 2006 (M_L7.1) Henchun earthquake occurred beneath southern Taiwan. The total available OBS data set consists of ~700 detected earthquakes, from which around 500 could be well located where about 450 events have been used in simultaneous inversion for hypocenters, three-dimensional Vp and Vp/Vs models for the study area. The main objective of incorporating gravity analysis is used to improve the velocity model for the offshore area, where it is poorly sampled by local earthquakes. This study found a low-velocity zone existing above the subducting South China Sea slab in the mantle wedge. Based on gravity modeling and our resulting velocity and Poisson's ratio models suggest that the subduction complex, which is characterized with a low P-wave velocity and low Poisson's ratios beneath the southern Taiwan. This duplex structure is characterized by a zone of low P-wave velocities in the range of 6.2–6.8 km/s between 25 and 40 km depth. It also shows that earthquake hypocenters do not fall within this low velocity zone. We have also used seismic tomography velocities to estimate the volume percentage of serpentinite and silica concentrations in southern Taiwan. The calculated serpentinite is about 30% and the volume percentage of quartz estimated is about 20% at the base of the forearc lower crust.

1. Introduction

It is generally believed that the tectonic evolution of Taiwan is a dynamic process on both time and space. Tectonic processes in Taiwan are characterized by an active orogeny between two subduction systems, the Ryukyu arc and the Luzon arc to the northeast and south, respectively. Between Taiwan and Luzon islands, the South China Sea lithosphere has been subducting eastward beneath the Philippine Sea Plate along the Manila Trench. The Manila subduction system progressively evolves from normal subduction to initial collision of the Taiwan orogen (e.g. Chemenda et al., 1997; Malavieille et al., 2002). This arc-trench system can be well perceived in the area south of ~21°N. North of ~21°N, the Manila trench loses its morphological characteristics and is replaced by the deformation front of the Taiwan region (Liu et al., 1997). Kao et al. (2000) used the bathymetry, seismicity, and source parameters of earthquakes and concluded a transition from oblique subduction to regional collision. According to Seno et al. (1993) and Yu et al. (1997), collision is propagating southwestward at ~5.5 cm/yr to eventually close the South China Sea (Fig. 1). The collision has uplifted the existing accretionary prism and forms the foreland basin in western Taiwan (e.g. Suppe, 1981; 1984; Chou and Yu, 2002).

Major large earthquakes frequently occur at subduction plate boundaries, as illustrated by the December 2004 Sumatra earthquake (Lay et al., 2005). Detailed knowledge of where subduction megathrusts rupture in earthquakes is critical for understanding the hazards associated with subduction megathrust earthquakes, and the physical processes behind subduction zone seismogenesis (e.g., Hyndman et al., 1995; Wallace et al., 2004; Bangs et al., 2006). The 26 December 2006 Pingtung earthquake (M_L = 7.1 in the USGS catalog, Fig. 1) and historical records of seismicity had prove that the actively deforming accretionary wedge is capable of generating large and probably great earthquakes. Recently the USGS issued a report assessing the potential risk as a tsunami source along the entire Pacific subduction zones and identified the Manila trench as a high risk zone. In southern Taiwan, significant progress has been made over the last decade to understand of the seismogenic potential and tectonics of the subduction zone (e.g., Kao et al., 2000; Lallemand et al., 2001; Liu et al., 2004; McIntosh et

* Corresponding author. Tel.: +886 2 82122000x6597; fax: +886 2 82122559.
E-mail addresses: wbin@just.edu.tw (W.B. Cheng), hsu@ncu.edu.tw (S.K. Hsu), gensin@scman.cwb.gov.tw (C.H. Chang).

0921-8181/$ – see front matter © 2012 Elsevier B.V. All rights reserved.
doi:10.1016/j.gloplacha.2012.01.003

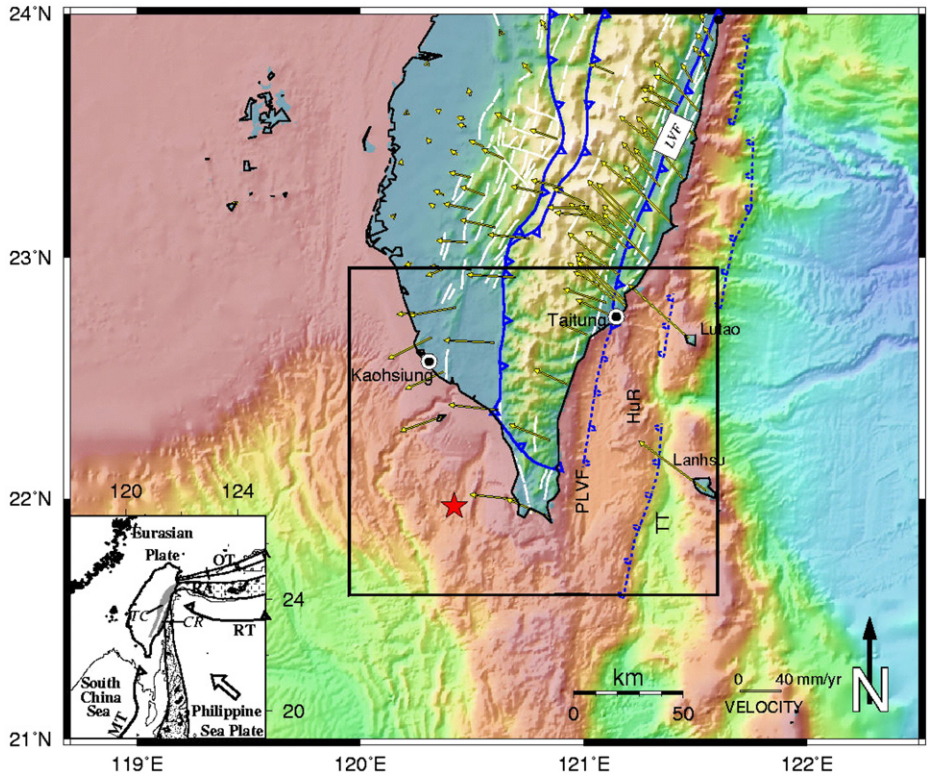

Fig. 1. Tectonic sketch map and bathymetry of the Taiwan region and location of the sections (geodynamic setting in the bottom-left). Solid square indicates the study area. Major thrust faults with open triangles on the upper side. Arrows indicate velocities of GPS stations relative to Penghu (Yu et al., 1997). Several thrust faults located in the eastern Taiwan offshore area are proposed by Malavieille et al. (2002). Solid red star indicates the epicenter of 2006 Pingtung earthquake. HuR—Hengchun Ridge; MT—Manila Trench; LA—Luzon Arc; LVF—Longitudinal Valley fault; OT—Okinawa Trough; PLVF—southern prolongation of Longitudinal Valley fault; RA—Ryukyu Arc; SLT—Southern Longitudinal Trough; TT—Taitung Trough.

al., 2005; Wu et al., 2007; Ku and Hsu, 2009; Lin et al., 2009). However, because of the lack of historical subduction thrust earthquake, little attention has been given to the points of the geometry and nature of the seismogenic zone, the plate interface, and the images of the Luzon mantle wedge.

The purpose of this paper is to present an iterative algorithm to correlate seismic travel-times and gravity data to obtain an optimum three-dimensional velocity structure of the subduction zone in southern Taiwan and (1) to investigate the velocity structure down to the plate boundary and mantle wedge using earthquake data, (2) to compare the structure off southern Taiwan obtained in this study with the seismicity, and (3) to discuss possible paths for fluid migration from deeper part to shallow crust. In this study, S–P arrival time data also used to obtain a Vp/Vs velocity model and to calculate the corresponding Poisson's ratios. It is expected that modeling the Poisson's ratio may provide further constrains on the lithologic and petrologic interpretation.

2. Data and analysis

2.1. Travel-time database

The earthquake data used in this study are P- and S-wave travel times of local earthquakes recorded by the Central Weather Bureau Seismographic Network (CWBSN). The earthquakes were selected to provide a set of hypocenters with high quality and best available ray coverage of the study area. They are reliable earthquake recordings recorded by the CWBSN during 1990 to 2008. In order to represent the full spatial distribution of the arrival data, offshore events with at least 6 high quality P arrivals were included that improve the spatial distribution of the data set. In addition to the CWBSN data set, the Pingtung earthquake (solid star in Fig. 1) occurred on December 26, 2006 provided well path coverage in this region and is extremely helpful in enhancing the resolution of tomography inversions and in accurately determining the locations of the aftershocks. Immediately following the occurrence of this event, a temporary network of 11 OBS instruments was deployed in the epicentral region from Dec. 27, 2006 to Jan. 3, 2007 in order to monitor the aftershocks. The seismicity related to these double earthquakes has been the largest earthquake sequence in this region in the past one hundred years. In this study, 47,125 P-arrivals and 31,314 S-arrivals from 3238 earthquakes were used. In order to refine the hypocenter and determine a more reliable one-dimensional (1-D) velocity model, the VELEST program (Kissling et al., 1994) was employed. The initial 1-D velocity model is modified from (Cheng, 2004; McIntosh et al., 2005; Liao et al., 2008; Cheng, 2009).

In this study, observed gravity is incorporated as a sequential step in the velocity inversion process developed by Parsons et al. (2001) was adapted in this study. First, the 3-D velocity model for the study area is obtained with the tomographic algorithms SIMULPS12 (Evans et al., 1994) based on the inversion method by Thurber (1983), Eberhart-Phillips (1990), and Thurber and Eberhart-Phillips (1999). We used the damped least squares inversion based on the parameter separation techniques of Pavlis and Booker (1980). The gravity anomaly is calculated on the first iteration of the velocity model by converting velocity to density using Gardner's non-linear rule of $\rho = 1740 V_p^{1/4}$ in grid nodes for velocities smaller than 6 km/s (Gardner et al., 1974). In considering the velocity anomalies greater than 15 km depth were resolvable using only seismic traveltimes, the velocity–density correlation gives rise to, a density value of 2.67 g/cm^3 for the middle crust (6.0–6.5 km/s), 2.85 g/cm^3 for the lower crust (6.5–7.0 km/s). A density of 3.0 g/cm^3 has been assumed for velocity greater than 7.0 km/s in the lower crust. The gravity anomaly resulting from the velocity model can be calculated by

converting velocities of the 3-D velocity model to densities. Then, the gravitational field predicted by the velocity model calculated from the travel-time inversion is compared with observed gravity. The residual between predicted and observed anomalies is minimized by weighted adjustments to the velocity model.

2.2. Solution quality

We used the checkerboard resolution test (CRT) proposed by Zhao et al. (1992) to assess resolution in specific regions and reliability of the 3-D model. We used the same procedures and parameters in the CRT inversions as those used in the inversions of real data. The synthetic velocity model was described by varying the velocity as a sinusoidal function in the x- and y-directions with alternating increase gradients that were ±10% over a background velocity between two adjacent nodes (Fig. 3). In addition, vertical gradients at various depths were also alternated to test the resolution of horizontal velocity boundaries. Synthetic traveltimes were calculated from each selected hypocenter to the recording stations through the checkerboard velocity models with random noises corresponding to phase-picking errors (a standard deviation of 0.1 s for the P wave and 0.15 s for the S wave). In the synthetic modeling, we fixed the coordinates of sources and treated them as artificial sources to calculate the synthetic travel-times. Ray tracing is accomplished using an approximate 3-D algorithm with curved nonplanar raypaths (Um and Thurber, 1987). Then, using a homogeneous initial model, synthetic data were then inverted using the same procedures applied to the actual stations and hypocenters. On the other hand, the synthetic gravity field was calculated with a model of 10×10 km columns, each with alternating increasing velocity gradients that were 0.5 m/s variant at all depths. The synthetic travel-times and synthetic gravity field were then used with a 1-D initial velocity model to recover the checkerboard pattern following a similar procedure suggested by Parsons et al. (2001). It indicates that the resolution of the Vp velocity structure is good in the onshore regions where seismic ray coverage is high. Significant improvement can be made by combining gravity data, particularly in areas of the offshore region (Fig. 4). This test suggests the utility of combining gravity data in the inversion, especially in studied areas with less ray coverage.

2.3. Recovery of the gravity anomaly

The CRT method can be used to investigate the spatial resolution provided by the existing ray coverage. On the other hand, the objective to incorporate gravity analysis is that the very limited coverage of seismic raypaths on velocity model. Gravity observations can add constraints to seismic images, at least to the extent that P-wave velocities of rocks can be estimated from their density (e.g. Roecker et al., 2004). Because of differences in sampling and sensitivity, sequentially satisfying seismic traveltime and observed gravity residuals in an iterative 3-D inversion can improve the accuracy and resolution of models derived independently. In general, seismic and gravity methods complement each other in various ways. Gravity anomalies increase in amplitude and decrease in wavelength with decreasing source depth. In addition, gravity anomalies are sensitive to lateral variations in density distribution. On the other hand, seismic methods are effective in resolving vertical variations. Thus, gravity inversions have greatest resolving power at shallow depths, where earthquake tomography is typically less effective, especially for the coastal and offshore areas. Fig. 4 shows a comparison of the gravity field calculated from velocity models developed with and without incorporating gravity analysis. Gravity data used in this study was compiled around Taiwan by Hsu et al. (1998). The residual between calculated and observed gravity is minimized by weighted adjustments to the model velocity–depth gradient where the gradient is steepest and where seismic coverage is very limited. After 4 iteration of calculation, we yielded a 3.4 mGal RMS misfit to the gravity. As expected, the gravity field for the offshore area calculated with gravity and seismic travel-times generates more features of the observed gravity anomalies than that of the seismic data only. In addition, adding a gravity constraint, as a sequential step in the seismic-velocity inversion, can highlight regions of the crust that have lateral velocity–density relations and significantly improve the resolution of the velocity structure in coastal area, southern Taiwan. With adding gravity data, however, the improvement is primarily recovery of the shape and scale of relative velocity variation rather than recovery of absolute velocities because a fixed velocity–density relation was used.

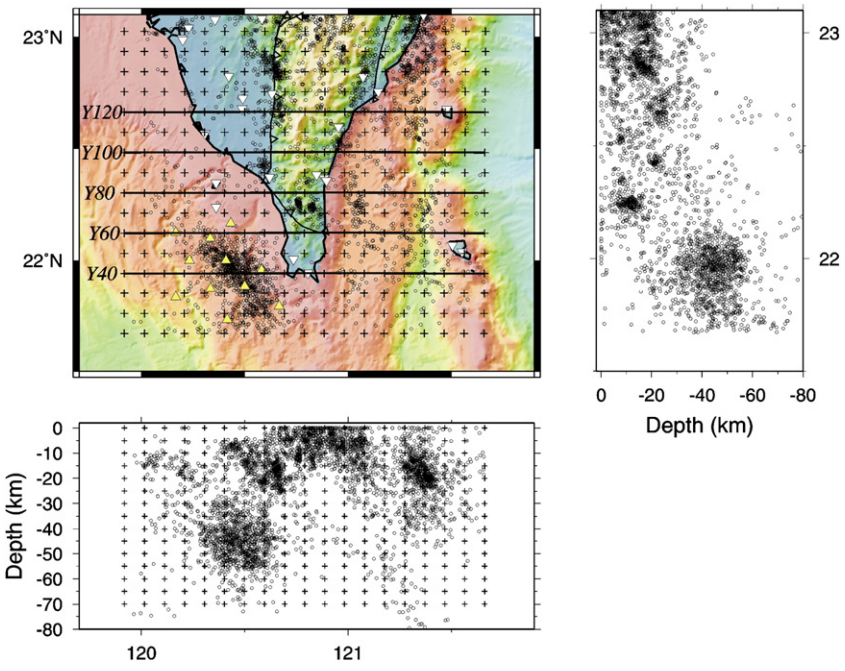

Fig. 2. (a) Grid nodes (crosses) and earthquakes (open circles) used in the three-dimensional inversion. Inverted open triangles denote permanent stations of the Central Weather Bureau Seismographic Network. Yellow triangles represent Ocean bottom seismographs. Location of velocity profiles Y40 to Y120 are shown in Fig. 6.

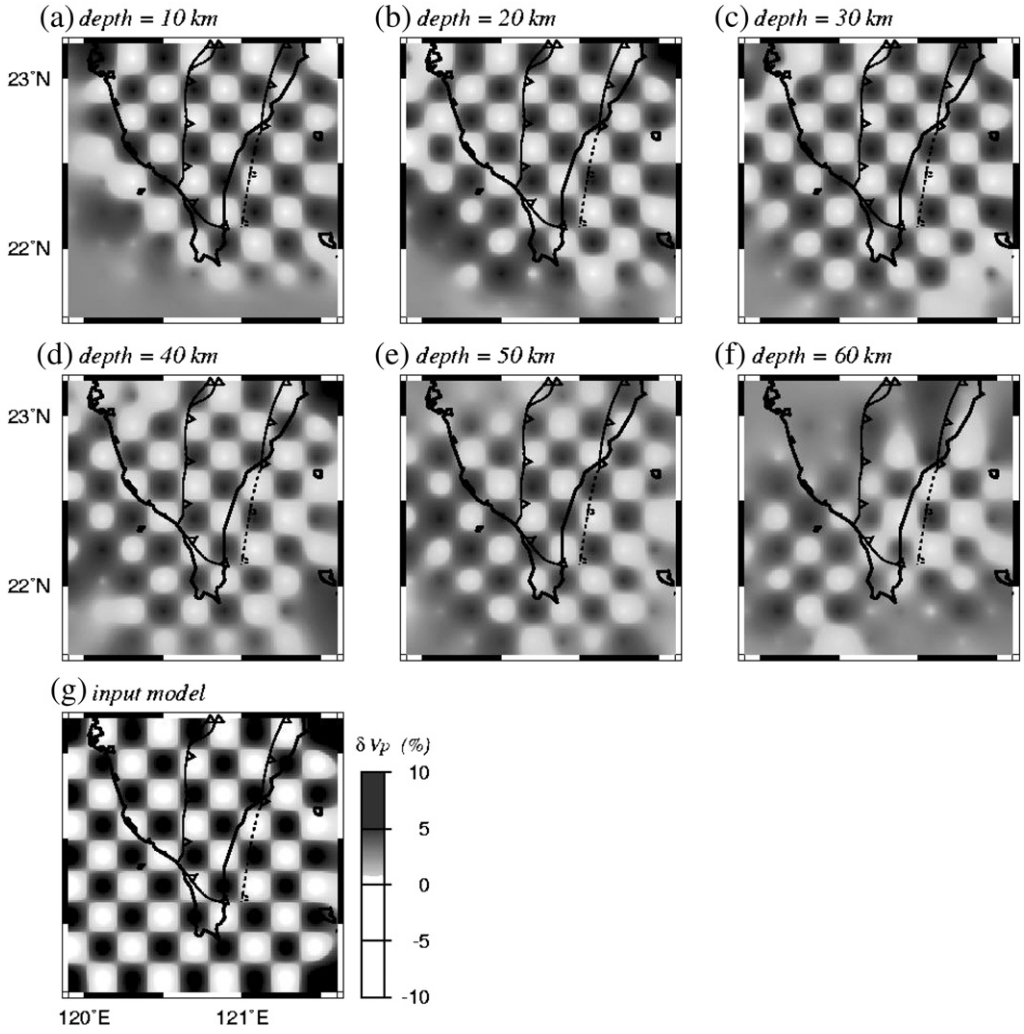

Fig. 3. Checkerboard resolution tests for P-wave model. The models recovered using seismic traveltimes are shown from 10-km to 60-km in depth.

3. Results and discussion

We plot a series of depth slices through the Vp and VpVs (Fig. 5), and vertical cross sections of the Poisson's ratios (σ) parallel to the latitude of southern Taiwan (Fig. 6). About 29,720 events with magnitude ≥2.0 recorded from 1991 to 2008 were relocated with the final 3-D velocity model. The hypocenters of the events used in the inversion within a 10-km distance from each cross section are also plotted. Chou et al. (2009) pointed out that the Vp/Vs anomaly is simply the difference between the Vp and Vs anomalies in

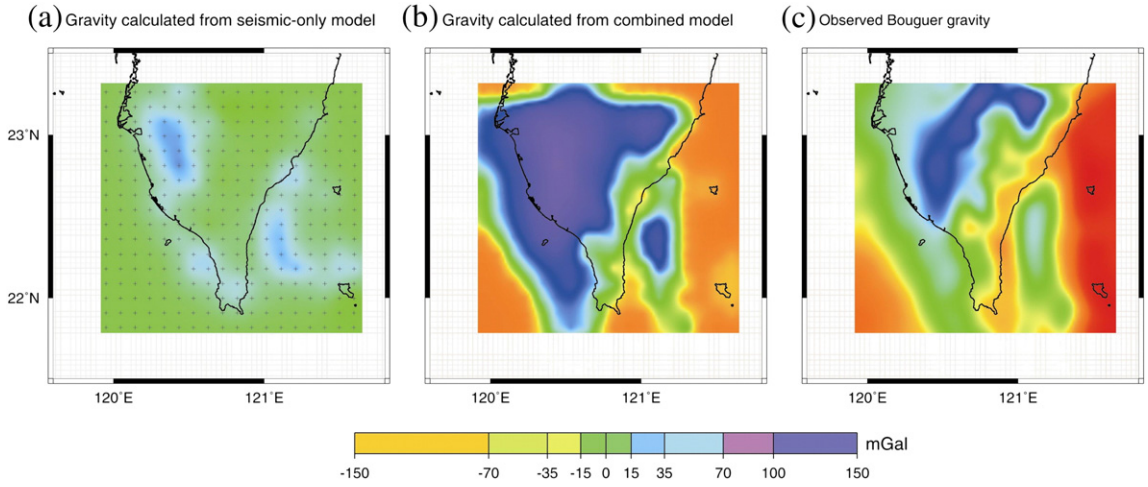

Fig. 4. Results of calculated gravity anomaly from velocity models obtained from: (a) seismic traveltimes only; (b) integrated seismic and gravity, and (c) observed gravity anomaly. It shows that more features of the observed gravity anomaly are apparent from the integrated analysis.

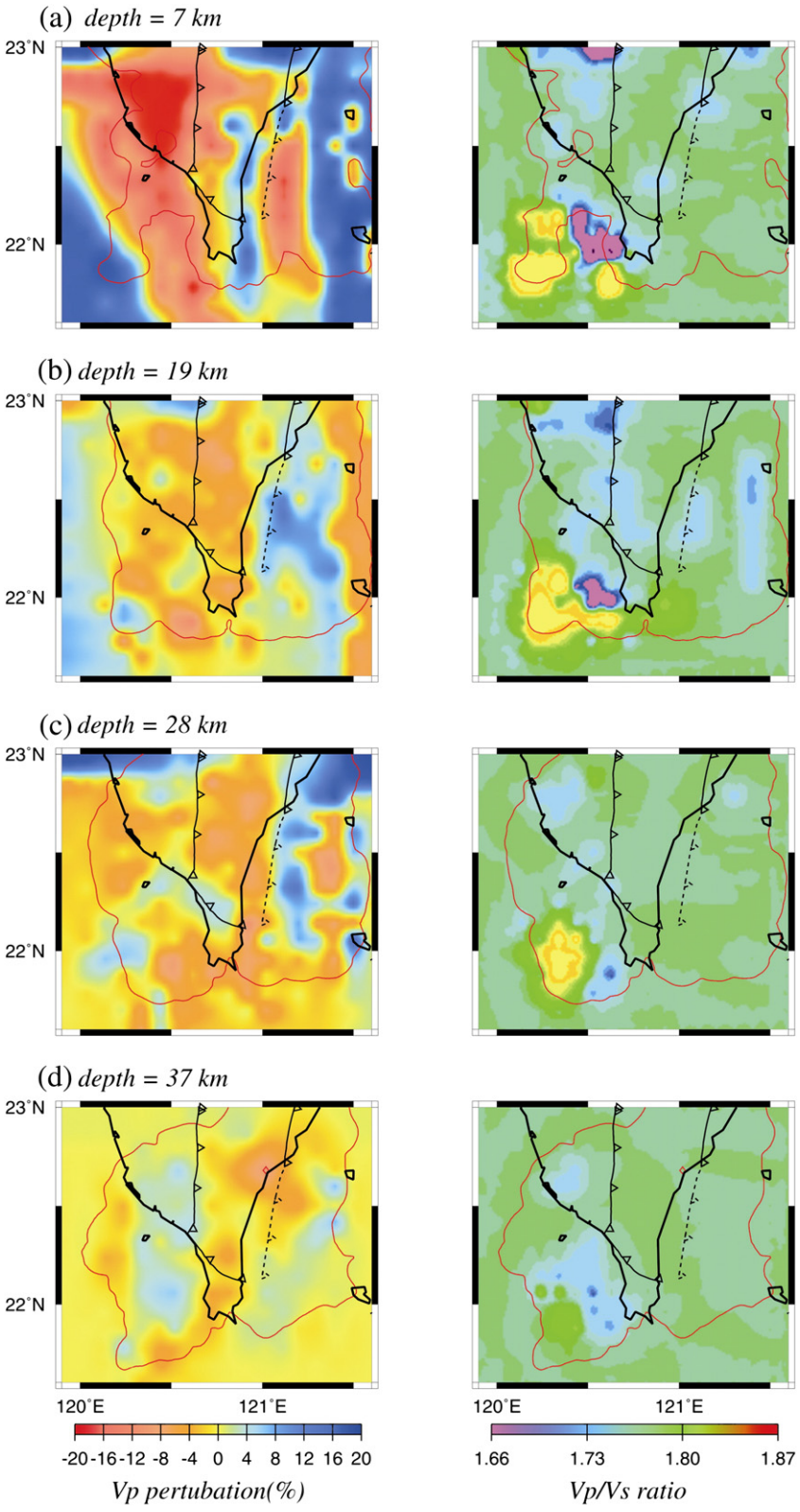

Fig. 5. Depth sections through the P-wave model (left) and Vp/Vs (right) labeled according to depth relative to sea level over shaded relief. Note that the velocities represented by the colors change with depth. Structure inside the red dashed line is meaningful, where the DWS for each node exceeds 100.

fractional form. Vp variations and σ can be grasped more intuitively and the algebraic summation of the results from two independent inversions for Vp and Vs (e.g. Walck, 1988). In addition, Poisson's ratios are also a useful tool for the interpretation in petrological terms (Christensen, 1966). Such estimates are nonunique, since several rock types often satisfy a particular Vp and σ.

It is known that the Poisson's ratios offer a means to distinguish between felsic (quartz rich) and mafic (quartz poor) crystalline

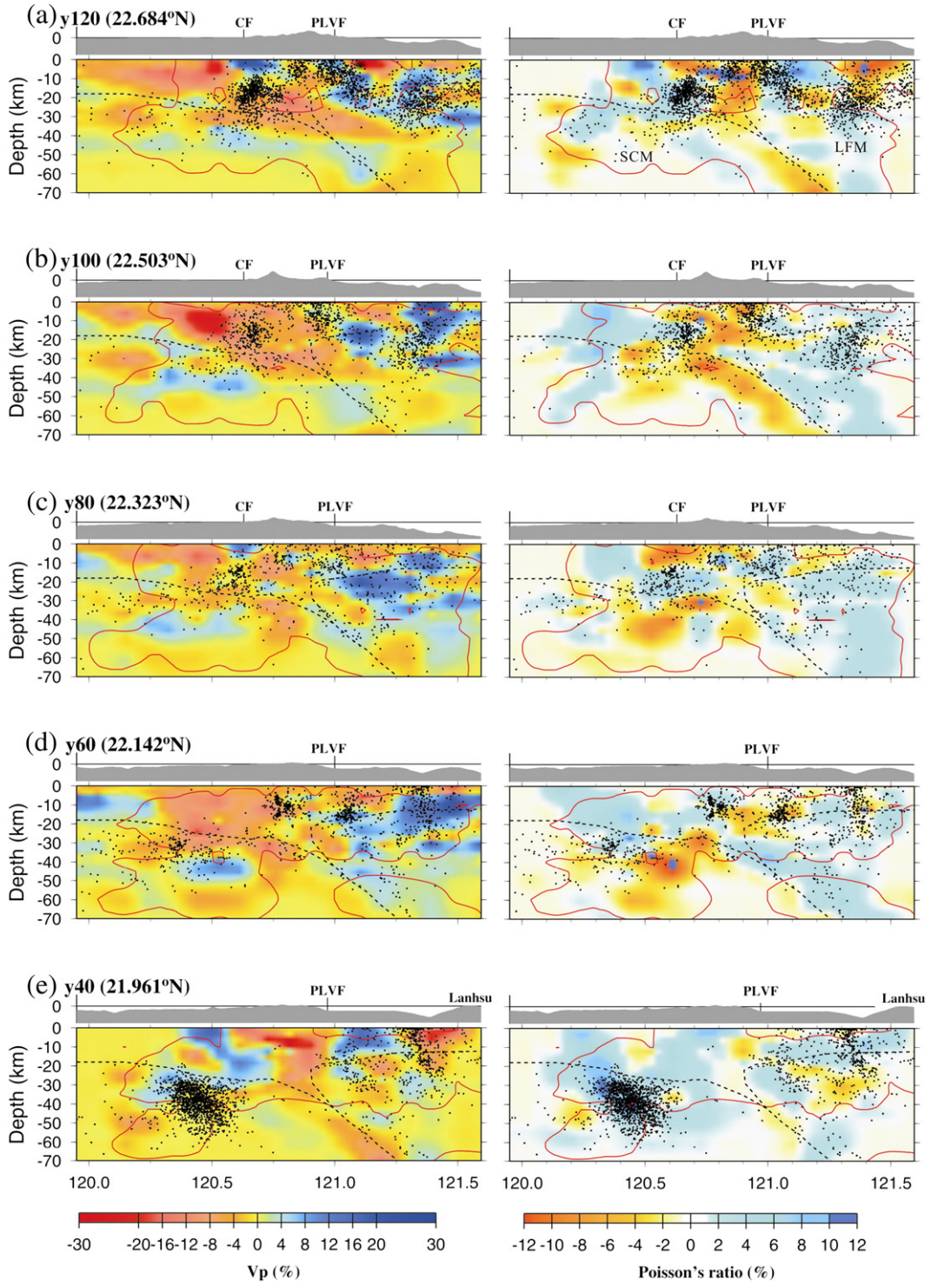

Fig. 6. Vertical cross-sections of P-wave velocity (left) and Poisson's ratio (right) along profiles from (a) north (Y120) to (e) south (Y40) sections as shown in Fig. 2. Blue and red denote fast and slow velocities, respectively. Topography of each section is shown on top. Open circles indicate relocated hypocenters. Dashed block delineate main tectonic units proposed for Luzon forearc mantle wedge on the right and South China Sea mantle on the left. Structure inside the red dashed line is meaningful, where the DWS for each node exceeds 100. CF—Chaozhou fault; PLVF—southern prolongation of Longitudinal Valley fault. LFM—Luzon forarc; SCM: South China Sea.

rocks (e.g. Holbrook et al. 1992). High values are expected for mafic and ultramafic rocks, and minerals having relatively high Poisson's ratios common in such rocks include plagioclase, amphibole, pyroxene and Fe-olivine (Musacchio et al., 1997). Therefore, the high-σ rocks observed at depth in the offshore area can be interpreted as the mantle wedge of the Luzon forearc (LFM) and South China Sea (SCM) from east to west, respectively (seen clear in Fig. 6b).

Between the mantle wedge of the Luzon forearc and South China Sea, a broad zone of low-σ and low Vp (6.2–6.8 km/s) is imaged in the lower crust, between 25 and 40 km depth beneath southern Taiwan on the vertical cross sections y60 to y120 (Figs. 6). It also shows that earthquake hypocenters do not fall within this low velocity zone. From these cross sections, we infer that the low-velocity rocks as the subduction complex underthrust the southern Taiwan

(Figs. 5 and 6). The eastward underthrusting of the low-velocity rocks of subduction complex might also deform the overlying crust and is probably the source of some seismicity in the depth range of 10 to 30 km. The low-velocity rocks of subduction complex exhibit a sharp velocity contrast with the neighboring rocks, as can be clearly observed on cross sections y60 to y100 in Fig. 6. In addition, the results show that the Poisson's ratios for the subduction complex are approximately 7% lower than those at the Luzon forearc mantle. Low Poisson's ratios, together with relatively low Vp, has been widely interpreted as indicative of hydration of the mantle or in situ melt retention. Hacker et al. (2003) pointed out that water release from the oceanic crust during descending may be absorbed by adjacent mantle peridotite and transform it to serpentine. In this study, we have also used seismic tomography Vp and Vp/Vs models in southern Taiwan to estimate the volume percentage of serpentinite and silica concentrations. We take the laboratory measurements of seismic velocities for peridotite serpentinized to various degrees from Christensen (1966) and Christensen (2004). Hyndman and Peacock (2003) also proposed a relationship between Vp, Vs, and volume percentage of serpentine. Fig. 7 shows volume percentage of serpentine along profile Y100.

As can be seen in Figs. 5 and 6, the lateral discontinuous change, i.e. the westernmost of the subduction complex in the crustal structure is coincident with the 2006 Pingtung earthquake source regions. The coincidence of the major focal regions and the structure with relatively lower Vp in the lower crust might have a number of explanations. The first is the possibility of a subducting seamount with the penetration of the South China Sea Plate. The subduction of a seamount might form a highly irregular interface, implying clustered asperities. When the subducting seamount reaches a certain depth, they might crash due to mechanical compaction with free water being released into the upper layer. The rising silica-saturated fluid has been released from the downgoing plate. Free water released by a collapsing seamount could decrease the P-wave velocities in the crust. With the addition of free water, peridotite in the mantle produces serpentines, which have velocities as slow as 6.2–6.8 km/s as obtained in this study. Measurements of seismic velocities in the laboratory show that velocities and densities of serpentinized peridotites vary from 4.9 to 7.4 km/s (Gebrande, 1982). An alternative explanation is that fluids released from the dehydration reactions occurring in the subducting slab can be trapped at this depth level and account as seismic E reflectors (Clowes et al., 1987; Hyndman, 1988; Calvert and

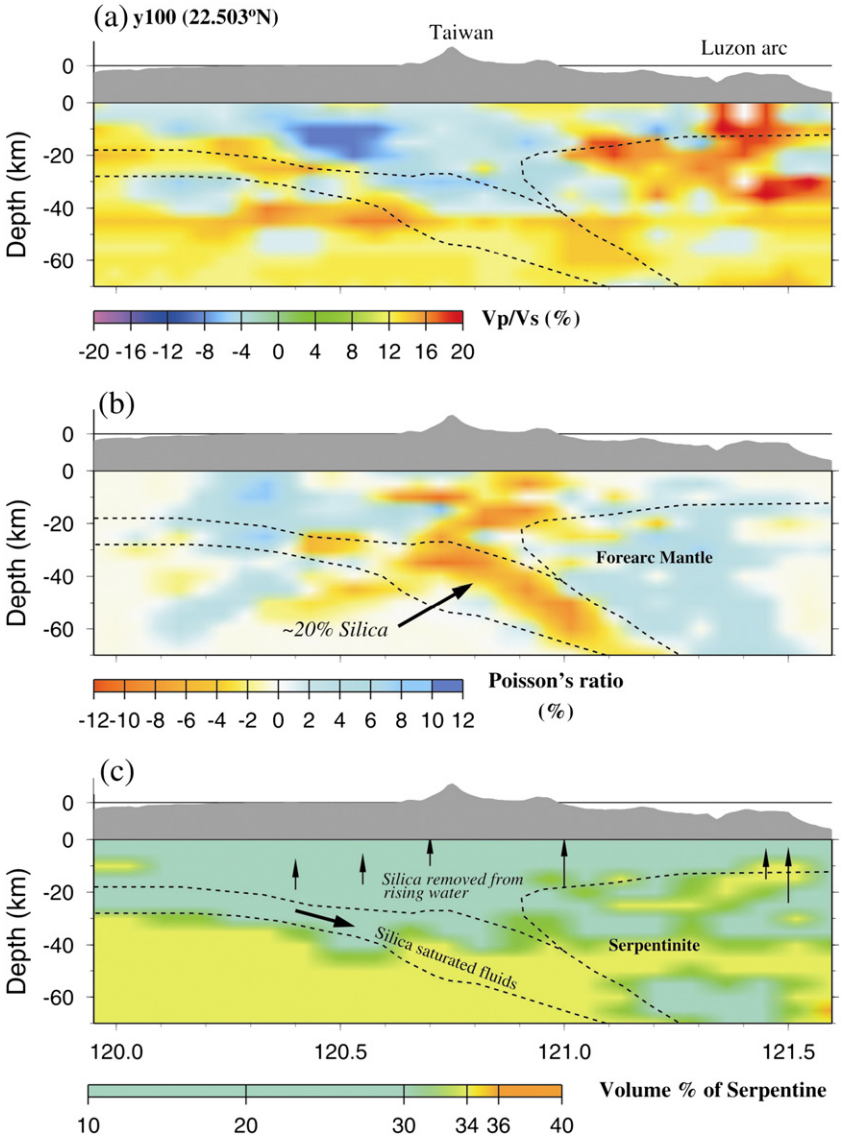

Fig. 7. Silica and serpentinite in subduction forearc. (a) Vertical cross-sections of Vp/Vs model. (b) Using a quartz with Poisson's ratio ~0.01 and normal lower crust values of 0.26, the volume percentage of quartz estimated is about 20%. (c) Calculated serpentinite and silica (~20%) concentrations along Y100 profile in southern Taiwan. The rising silica-saturated fluid has been released from the downgoing plate.

Clowes, 1990). In Fig. 7, the low velocities imaged between 25 and 40 km depth beneath southern Taiwan coincides with the zone of postulated mechanisms of shearing, and presence of fluids (Hyndman, 1988). One may notice that earthquake hypocenters do not fall within this low velocity zone in southern Taiwan (Fig. 6). One explanation for it may be that any accumulated stress there is probably released by episodic, aseismic slow-slip events (e.g. Dragert et al., 2001; Hirose and Obara, 2005; Shelly et al., 2006). The episodic tremors are distributed over a wide depth range of 40 km with a peak at 25–35 km beneath Vancouver Island. Calvert and Clowes (1990) reported that >90% of the local earthquakes tend to be located away from the E reflectors.

Lin et al. (2009) pointed out that vigorous fluid expulsion, a sign of the existence of high pore-pressure zones were observed in the offshore accretionary belt, southwestern Taiwan. For example, widespread occurrence of bottom simulating reflectors, indicates the presence of gas hydrates and thus sufficient supply of methane and water (Liu et al., 2006). The existence of an array of mud volcanoes (Chiu et al., 2006; Liu et al., 2006) and mud diapirism (Sun and Liu, 1993) reveals high methane content in seafloor sediments (Chuang et al., 2006). It is widely believed that high fluid pressure along the decollement fault zone plays an important role in many aspects of earthquake faulting and in the mechanics of accretionary wedges. Pore fluid pressure elevated above hydrostatic along thrust faults is a well established mechanism for reducing fault strength and enhancing thrusting (Hubbert and Rubey, 1991; Rice, 1992). Thrusting and thickening of fluid-rich sediments in accretionary wedge can continually increase the overburden load, squeezing out fluids and consolidating sediment caught in plate collision. Drilling studies of the Barbados Ridge discovered extensive evidence for fluids and a fluid flow system along the decollement plate boundary fault that accommodates a major portion of the fluid expulsion out of the subduction zone (Moore et al., 1988). In addition, fluids in accretionary wedge strongly affect the styles of deformation which result from plate convergence. In order to understand the relationship of upward expelled water with low-velocity serpentinite in the forearc mantle and low Poisson's ratio silica deposited at the lower crust, we have also used seismic tomography Vp and Vp/Vs models in southern Taiwan to estimate the silica concentrations. In this study, we know the Poisson's ratio of forearc crustal rock is normally in the range 0.21 to 0.29 for Mesozoic/Cenozoic orogenic belts (Zandt and Ammon, 1995). Using a quartz with Poisson's ratio ~0.01 and normal lower crust values of 0.26 (Zandt and Ammon, 1995), the volume percentage of quartz estimated is about 20% in subduction forearc (Fig. 7). Silica-rich rocks are not normally indicated in the lower crust, but they can be expected in the environment of the forearc (Manning, 1996). Breeding and Ague (2002) reported that quartz deposited in an exposed deep forearc section, from silica-rich fluids rising from the subducted slab. It is believed that solubility of silica is strongly temperature dependent (e.g. Peacock and Hyndman, 1999), most of the silica beneath southern Taiwan will be rapidly removed and deposited in the lower crust above the subducting South China Sea slab.

4. Conclusions

Our regional 3-D P-wave and Poisson's ratio models present the regional image of the southern Taiwan subduction zone. This study found a low-velocity zone existing above the subducting South China Sea slab in the mantle wedge. This duplex structure is characterized by broad zone of low P- wave velocities in the range of 6.2–6.8 km/s between 25 and 40 km depth. It also shows that earthquake hypocenters do not fall within this low velocity zone. Two possible interpretations of the coincidence of crustal structure heterogeneity are given, the first is seamount subducting beneath the southern Taiwan, and the second is emplacement of crustal rocks into the forearc mantle. We have also used seismic tomography velocities to estimate the volume percentage of serpentinite and silica concentrations in southern Taiwan. The calculated serpentinite is about 30% and the volume percentage of quartz estimated is about 20% at the base of the forearc lower crust. It is suggested that most of the silica beneath southern Taiwan will be rapidly removed and deposited in the lower crust above the subducting South China Sea slab.

Acknowledgments

The author is grateful to the Seismological Observation Center, Central Weather Bureau, for providing earthquake data. I am deeply indebted to Tom Parsons for making available his algorithm and I appreciate Drs. K. McIntosh, and T. Byrne for their valuable discussion. The research was supported by the National Science Council of Taiwan, under grant NSC100-3113-S-228-002 and NSC99-2116-M-228-001. The Editor, Sierd Cloetingh, and two anonymous reviewers provided helpful comments on the initial version of the manuscript. Some figures were generated by the GMT software written by Paul Wessel and Walter H. F. Smith.

References

Bangs, N.L.B., Gulick, S.P.S., Shipley, T.H., 2006. Seamount subduction erosion in the Nankai Trough and its potential impact on the seismogenic zone. Geology 34 (8), 701–704. doi:10.1130/G22451.1.
Breeding, C.M., Ague, J.J., 2002. Slab-derived fluids and quartz-vein formation in an accretionary prism, Otago Schist, New Zealand. Geology 30, 499–502.
Calvert, A.J., Clowes, R.M., 1990. Deep, high-amplitude reflections from a major shear zone above the subducting Juan de Fuca plate. Geology 18, 1091–1094.
Chemenda, A.I., Yang, R.K., Hsieh, C.H., Groholsky, A.L., 1997. Evolutionary model for the Taiwan collision based on physical modeling. Tectonophysics 274, 253–274.
Cheng, W.B., 2004. Crustal structure of the high magnetic anomaly belt, western Taiwan, and its implications for continental margin deformation. Marine Geophysical Researches 25, 79–93.
Cheng, W.B., 2009. Tomographic imaging of the convergent zone in eastern Taiwan — a subducting forearc sliver revealed? Tectonophysics 466, 170–183.
Chiu, J.K., Tseng, W.H., Liu, C.S., 2006. Distribution of gassy sediments and mud volcanoes offshore southwestern Taiwan. Terrestrial Atmospheric and Oceanic Sciences 17, 703–722.
Chou, Y.W., Yu, H.S., 2002. Structural expressions of flexural extension in the arc-continental collisional foredeep of western Taiwan. Geological Society of America Bulletin Special Papers 358, 1–12.
Chou, H.C., Kuo, B.Y., Chiao, L.Y., Zhao, D., Hung, S.H., 2009. Tomography of the western-most Ryukyu subduction zone and the serpentinization of the fore-arc mantle. Journal of Geophysical Research 114, B12301. doi:10.1029/2008JB006192.
Christensen, N.I., 1966. Elasticity of ultrabasic rocks. Journal of Geophysical Research 71, 5921–5931.
Christensen, N.I., 2004. Serpentinites, peridotites, and seismology. International Geology Review 46, 795–816. doi:10.2747/0020-6814.46.9.795.
Chuang, P.-C., Yang, T.F., Lin, S., Lee, H.-F., Lan, T.-F., Hong, W.-L., Liu, C.-S., Chen, J.-C., Wang, Y., 2006. Extremely high methane concentration in bottom water and cored sediments from offshore southwestern Taiwan. Terrestrial Atmospheric and Oceanic Sciences 17, 903–920.
Clowes, R.M., Brandon, M.T., Green, A.G., Yorath, C.J., Sutherland-Brown, A., Kanasewich, E.R., Spencer, C.S., 1987. LITHOPROBE southern Vancouver Island: Cenozoic subduction complex imaged by deep seismic reflections. Canadian Journal of Earth Sciences 24, 31–51.
Dragert, H., Wang, K., James, T., 2001. A silent slip event on the deeper Cascadia subduction interface. Science 292, 1525–1528. doi:10.1126/science.1060152.
Eberhart-Phillips, D., 1990. Three-dimensional P and S velocity structure in the Coalinga region, California. Journal of Geophysical Research 95, 15,343–15,363.
Evans, J.R., Eberhart-Philips, D., Thurber, C.H., 1994. User's manual for SIMULPS12 for imaging Vp and Vp/Vs: a derivative of the "Thurber" tomography inversion SIMUL3 for local earthquakes and explosions. U.S. Geological Survey Open-File Report 94–431 100 pp..
Gardner, G.H.F., Gardner, L.W., Gregory, A.R., 1974. Formation velocity and density: the diagnostic basis for stratigraphic traps. Geophysics 39, 770–780.
Gebrande, H., 1982. Elastic wave velocities and constants of elasticity of rocks at room temperature and pressures up to 1 GPa. In: Angenheister, G. (Ed.), Physical Properties of Rocks, 1. Springer, Berlin, pp. 35–99.
Hacker, B.R., Abers, G.A., Peacock, S.M., 2003. Subduction factory 1. Theoretical mineralogy, densities, seismic wave speeds, and H2O contents. Journal of Geophysical Research 108 (B1), 2029. doi:10.1029/2001JB001127.
Hirose, H., Obara, K., 2005. Repeating short- and long-term slow slip events with deep tremor activity around the Bungo channel region, southwest Japan. Earth, Planets and Space 57, 961–972.
Holbrook, W.S., Mooney, W.D., Christensen, N.I., 1992. The seismic velocity structure of the deep continental crust. In: Fountain, D.M., Arculus, R., Kay, R.W. (Eds.), The Lower Continental Crust. Elsevier Science, New York, pp. 1–43.

Hsu, S.K., Liu, C.S., Shyu, C.T., Liu, S.Y., Sibuet, J.C., Lallemand, S., Wang, C., Reed, D., 1998. New gravity and magnetic anomaly maps in the Taiwan–Luzon region and their preliminary interpretation. Terrestrial Atmospheric and Oceanic Sciences 9, 509–532.

Hubbert, M.K., Rubey, W.W., 1991. Role of fluid pressure in the mechanics of overthrust faulting, I, mechanics of fluid-filled porous solids and its application to overthrust faulting. Geological Society of America Bulletin 70, 115–166.

Hyndman, R.D., 1988. Dipping seismic reflectors, electrically conductive zones, and trapped water in the crust over a subducting plate. Journal of Geophysical Research 93, 13,391–13,405.

Hyndman, R.D., Peacock, S.M., 2003. Serpentinization of the forearc mantle. Earth and Planetary Science Letters 212, 417–432.

Hyndman, R.D., Wang, K., Yamano, M., 1995. Thermal constraints on the seismogenic portion of the southwestern Japan subduction thrust. Journal of Geophysical Research 100, 15,373–15,392. doi:10.1029/95JB00153.

Kao, H., Huang, G.C., Liu, C.S., 2000. Transition from oblique subduction to collision in northern Luzon arc-Taiwan region: constrains from bathymetry and seismic observations. Journal of Geophysical Research 105, 3059–3079.

Kissling, E., Ellsworth, W., Eberhart-Phillips, D., Kradolferet, U., 1994. Initial reference models in local earthquake tomography. Journal of Geophysical Research 99, 19635–19646.

Ku, C.-Y., Hsu, S.-K., 2009. Crustal structure and deformation at the northern Manila Trench between Taiwan and Luzon islands. Tectonophysics 466, 229–240.

Lallemand, S., Font, Y., Bijwaard, H., Kao, H., 2001. New insights on 3-D plates interaction near Taiwan from tomography and tectonic implications. Tectonophysics 335, 229–253.

Lay, T., Kanamori, H., Ammon, C.J., Nettles, M., Ward, S.N., Aster, R.C., Beck, S.L., Bilek, S.L., Brudzinski, M.R., Butler, R., DeShon, H.R., Ekstrm, G., Satake, K., Sipkin, S., 2005. The great Sumatra–Andaman earthquake of 26 December 2004. Science 308, 1127–1133.

Liao, Y., Hsu, S.K., Chang, C.H., Doo, W.B., Ho, M.Y., Lo, C.L., Lee, C.S., 2008. Seismic tomography off SW Taiwan: a joint inversion from OBS and onshore data of 2006 Pingtung aftershocks. Terrestrial Atmospheric and Oceanic Sciences 19, 729–741.

Lin, A.T., Yao, B., Hsu, S.-K., Liu, C.-S., Huang, C.-Y., 2009. Tectonic features of the incipient arc-continent collision zone of Taiwan: implications for seismicity. Tectonophysics 479, 28–42.

Liu, C.S., Huang, I.L., Teng, L.S., 1997. Structural features off southwestern Taiwan. Marine Geology 137, 305–319.

Liu, C.-S., Deffontaines, B., Lu, C.-Y., Lallemand, S., 2004. Deformation patterns of an accretionary wedge in the transition zone from subduction to collision offshore southwestern Taiwan. Marine Geophysical Research 25, 123–137.

Liu, C.-S., Schn rle, P., Wang, Y., Chung, S.-H., Chen, S.-C., Hsiuan, T.-H., 2006. Distribution and characters of gas hydrate offshore of southwestern Taiwan. Terrestrial, Atmospheric and Oceanic Sciences 17, 615–644.

Malavieille, J., Lallemand, S.E., Domingquez, S., Deschamps, A., Lu, C.Y., Liu, C.S., Schnurle, P., ACT Scientific Crew, 2002. Arc-continent collision in Taiwan: new marine observations and tectonic evolution. In: Byrne, T.B., Liu, C.S. (Eds.), Geology and Geophysics of an Arc-Continent collision, Taiwan: Geological Society of America Special Paper., 358, pp. 187–211.

Manning, C.E., 1996. Effects of sediments on aqueous silica transport in subduction zones. In: Bebout, G., Scholl, D.W., Kirby, S.H., Platt, J.P. (Eds.), Subduction Top to Bottom. American Geophysica Union, Wash., D.C, pp. 277–284. 1996.

McIntosh, K., Nakamura, T.Y., Wang, T.K., Shih, R.C., Chen, A., Liu, C.S., 2005. Crustal-scale seismic profiles across Taiwan and the western Philippine Sea. Tectonophysics 401, 23–54.

Moore, J.C., Mascle, A., Taylor, E., 1988. Tectonics and hydrology of the northern Barbados Ridge: results from Ocean Drilling Program Leg 110. Geological Society of America Bulletin 100, 1578–1593.

Musacchio, G., Mooney, W.D., Luetgert, J.H., 1997. Composition of the crust in the Grenville and Appalachian Provinces of North America inferred from Vp/Vs ratios. Journal of Geophysical Research 102 (B7), 15225–15241.

Parsons, T., Blakely, R.J., Brocher, T.M., 2001. A simple algorithm for sequentially incorporating gravity observations in seismic traveltime tomography. International Geology Review 43, 1073–1086.

Pavlis, G.L., Booker, J.R., 1980. The mixed discrete-continuous inverse problem: application to the simultaneous determination of earthquake hypocenters and velocity structure. Journal of Geophysical Research 85 (4801–85), 4810.

Peacock, S.M., Hyndman, R.D., 1999. Hydrous minerals in the mantle wedge and the maximum depth of subduction thrust earthquakes. Geophysical Research Letters 26, 2517–2520.

Rice, J.R., 1992. Fault stress states, pore pressure distributions, and the weakness of the San Andreas fault. In: Evans, B., Wong, T.-F. (Eds.), Fluid Mechanics and Transport Properties of Rocks. Academic Press, San Diego, Calif, pp. 475–503.

Roecker, S., Thurber, C., McPhee, D., 2004. Joint inversion of gravity and arrival time data from Parkfield: new constraints on structure and hypocenter locations near the SAFOD. Geophysical Research Letters 31, LS12S04. doi:10.1029/2003GL019396.

Seno, T., Stein, S., Gripp, A.E., 1993. A model for the motion of the Philippine Sea Plate consistent with NUVEL-1 and geologic data. Journal of Geophysical Research 98, 17941–17948.

Shelly, D.R., Beroza, G.C., Ide, S., Nakamula, S., 2006. Low frequency earthquakes in Shikoku, Japan, and their relationship to episodic tremor and slip. Nature 442, 188–191.

Sun, S.C., Liu, C.S., 1993. Mud diapirs and submarine channel deposits in offshore Kaohsiung-Hengchun, southwest Taiwan. Petroleum Geology of Taiwan 28, 1–14.

Suppe, J., 1981. Mechanics of mountain building and metamorphism in Taiwan. Memoir of the Geological Society of China 4, 67–89.

Suppe, J., 1984. Kinematics of arc-continent collision, flipping of subduction, and back-arc spreading near Taiwan. Memoir of the Geological Society of China 6, 21–33.

Thurber, C.H., 1983. Earthquake locations and three-dimensional crustal structure in the Coyote Lake area, central California. Journal of Geophysical Research 88, 8226–8236.

Thurber, C., Eberhart-Phillips, D., 1999. Local earthquake tomography with flexible gridding. Computers & Geosciences 25, 809–818.

Um, J., Thurber, C., 1987. A fast algorithm for two-point seismic ray tracing. Bulletin of the Seismological Society of America 77 (3), 972–986.

Walck, M., 1988. Three-dimensional Vp/Vs variations for the Coso region, California. Journal of Geophysical Research 93, 2047–2052. doi:10.1029/JB093iB03p02047.

Wallace, L.M., Beavan, J., McCaffrey, R., Darby, D., 2004. Subduction zone coupling and tectonic block rotations in the North Island, New Zealand. Journal of Geophysical Research 109, B12406. doi:10.1029/2004JB003241.

Wu, Y.M., Chang, C.H., Zhao, L., Shyu, J.B.H., Chen, Y.G., Sieh, K., Avouac, J.P., 2007. Seismic tomography of Taiwan: improved constraints from a dense network of strong-motion stations. Journal of Geophysical Research 112 (B8), B08312. doi:10.1029/2007JB004983.

Yu, S.B., Chen, H.Y., Kuo, L.C., 1997. Velocity field of GPS stations in the Taiwan area. Tectonophysics 274, 41–59.

Zandt, G., Ammon, C.J., 1995. Continental-crust composition constrained by measurements of crustal Poisson ratio. Nature 374, 152–154.

Zhao, D., Hasegawa, A., Horiuchi, S., 1992. Tomographic imaging of P and S wave velocity structure beneath northeastern Japan. Journal of Geophysical Research 97, 19909–19928.